# Experimental and numerical investigation of hydrogen injection, spontaneous ignition and flame stabilization in a lab-scale sequential combustor at high pressure

*Peter* Griebel[1,*], *Joshua* Gray[1], *Holger* Ax[1], *Oliver* Lammel[1], *Klaus-Peter* Geigle[1], *Ole H. H.* Meyer[2], *Andrea* Gruber[2,3], *Birute* Wood[4], *Michael* Düsing[4], *Andrea* Ciani[4]

[1] German Aerospace Center (DLR) Pfaffenwaldring 38-40, 70569 Stuttgart, Germany
[2] SINTEF Energy Research, 7465 Trondheim, Norway
[3] Norwegian University of Science and Technology, 7491 Trondheim, Norway
[4] Ansaldo Energia Switzerland, Haselstrasse 18, 5400 Baden, Switzerland
* Lead author

**Abstract.** Sequential combustion staging has emerged as a well-suited approach for burning hydrogen in gas turbines, while maintaining low emissions and high cycle efficiency. A characteristic feature of sequential combustion systems is the high inlet temperature and the balance of flame propagation versus spontaneous ignition controlling flame stabilization in the second combustor stage. For the development of gas turbine combustion systems, able to operate on carbon-free fuels, it is important that experimental data at relevant conditions is available and that turbulent combustion models can accurately predict flame stabilization in the highly turbulent reacting flow. To match the propagation-to-auto-ignition balance, which is controlling flame stabilization, experimental validation of numerical models plays a key role in combustion systems development. Experimental results of $N_2$-diluted hydrogen and pure hydrogen flames serve as a validation basis of Large-Eddy Simulations. Two flame stabilization configurations are investigated featuring significant differences in the steady-state flame location. Flame stabilization occurs in the combustor or directly at the fuel injection nozzle. The numerical model tested is able to capture the main flame-stabilization location observed in the experiments, while it is unclear whether the model correctly captures the occurrence of intermittent small ignition kernels in the mixing section.

## 1 Introduction

Decarbonisation of the power sector is key in the ongoing efforts to mitigate climate change. The envisioned zero-emissions society targets to include a blend of multiple renewable energy systems and energy carriers, such as hydrogen ($H_2$) or ammonia ($NH_3$). At any rate, security of supply and efficient use/distribution of electric power pose constraints on the availability of intermittently available power generators. The future's energy system will likely rely on a mixture of different carbon reduced or carbon free fuels, such as natural gas (with CCS) or hydrogen. Swift transition to a decarbonised energy system mandates cost-effective solutions, preferably of a high degree of retrofittability to pose attractive alternatives in terms of investment costs. To this end, a re-purposable, fuel-flexible combustion system, free from constraints on fuel purity, and high operational flexibility, is clearly desired to adapt to varying degrees of fuel availability and enable grid balancing.

The *reheat concept* is able to provide fuel-flexibility, by varying loading of each of the two sequential combustor stages separately, allowing stable operation of highly reactive fuels (such as hydrogen) in the first stage at lower flame temperature compared to natural gas operation, and high hydrogen fuel contents to be burned efficiently in the second stage, conserving engine rating [1, 2]. Typically, the sequential combustor is subject to pressures exceeding 10 bar, high reactant temperatures above 1000 K and the presence of vitiated oxygen ($O_2$). As part of ongoing research to develop computational tools that can reliably predict reheat combustion processes for arbitrary hydrogen contents, experimental validation of the numerical models is crucially required.

Experimental studies on a geometrically simplified sequential combustor under reheat conditions, studying the formation of auto-ignition (AI) kernels for cross-flow and inline fuel injection, have been performed by DLR over a period spanning more than a decade [3, 4, 5, 6, 7]. Together with the aforementioned early experimental work, more recent measurements of hydrogen injection under reheat conditions in a slightly modified sequential combus-

tor are obtained to serve as a database for model validation. Improving upon and learning from the earlier study [7], the new experiments exploit an optimized thermocouple probe and a sequential combustor exit section with a converging cross section. Otherwise, these follow a similar approach as earlier experimental campaigns performed at DLR, specifically, employing geometric setup and operational configurations as detailed in [5] and references therein.

In the literature, simplified numerical studies considering hydrogen and methane ($CH_4$) combustion at reheat conditions have been performed, mostly to aid detailing of full-scale, high pressure experiments [2, 8, 9]. Quantification of the relative importance of flame spontaneous ignition vs flame propagation has been attempted by applying Direct Numerical Simulation (DNS) [10] and Large-Eddy Simulation (LES) [11] to simple laboratory flames. Moreover, LES has been applied to study a reheat sequential combustor at atmospheric pressure fueled by methane [12] while the dynamic response of AI stabilized flames has been investigated using LES to extract the flame transfer function [13, 14, 15]. Additional DNS studies have shed light on the physical characteristics of hydrogen-air combustion under atmospheric and mildly-pressurized reheat conditions [16]. Using LES, hydrogen reheat flames stabilized in a geometrically-simplified combustor subject to pressure variations from part-load and to full-load conditions representative of the Ansaldo Energia's GT26/GT36 sequential combustion system have been studied assuming homogeneous mixing [17]. In that work, synthetic turbulence-like fluctuations were applied at the domain inlet boundary and the mixing channel length was assessed in respect to the spatial development of the turbulent and thermal boundary layers with significant impact on flame stabilization [17]. A follow-up study performed massively-parallel LES of a 30-degrees sector of the actual Ansaldo Energia's GT36 sequential combustion system [18]. Although this effort resulted in promising outcomes in terms of the model's ability to predict fuel injection, mixing with the vitiated oxidizer stream and spontaneous ignition of the reactants mixture at the expected stabilization location, the study lacked a solid validation base for the numerical simulations [18].

The present work tries to address the issue of model validation by providing a more complete experimental base compared to what is available from typical rig testing of the industrial combustion system while still incorporating realistic turbulence and scalar fields transitioning from non-premixed to partially premixed covering the range of conditions present in industrial combustors. In the configuration investigated, the turbulence is generated by the interaction of the high-speed flow of the hot gas with the fuel-injector geometry, which acts as a bluff body. Resolving the fuel and carrier air injection characteristics as they interact with the hot gas, we simulate in detail the spatial evolution of the three-streams mixing field ultimately leading to the stabilization of the hydrogen reheat flame. We consider both nitrogen-diluted hydrogen ($H_2/N_2$ mixture) and pure hydrogen fuel. For the nitrogen-diluted hydrogen flames, we perform two numerical simulations, aiming to replicate the salient features from the experiments in terms of qualitative measures for AI kernel generation and flame-anchoring position. The two cases are classified as low-hydrogen content, corresponding to part-load engine operation, and high-hydrogen content, corresponding to full-load conditions. For the pure-hydrogen flames, we perform simulations with different inlet temperature of the hot gas, testing the model ability to qualitatively predict the characteristic flame-anchoring behavior observed in the experiments.

# 2 Experimental setup, numerical model and configuration

## 2.1 Experimental setup

The experiments were performed in an optically accessible simplified sequential combustor (SC), which was integrated in the high-pressure combustion rig HBK-S at DLR Stuttgart. A sketch of the combustor concept is shown in fig. 1 (top). It consists of three main sections: A natural gas fuel stream is burned in a jet-stabilized burner in the first combustor stage and diluted with air at ambient temperature to form the hot gas stream. The hot gas generator (HG) is delivering hot flue gas at temperatures and gas compositions typical for sequential combustors. In the subsequent mixing section (MS), fuel ($H_2/N_2$ mixtures or $H_2$) is injected together with preheated curtain air into the hot gas stream. The fuel/carrier air/hot gas mixture is then burned in the sequential combustor (SC).

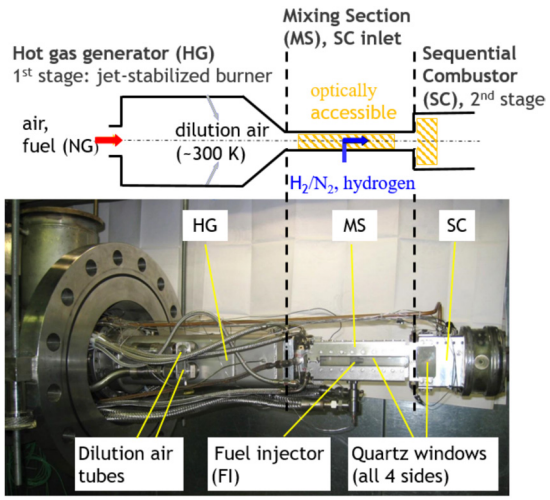


**Fig. 1:** Concept (top) and photo of the 2-stage combustor (bottom).

A schematic of the fuel injector (FI) is presented in fig. 2. The fuel is injected with a FI, consisting of a central fuel jet, either a $H_2/N_2$ mixture or pure $H_2$, surrounded by a co-flow of so-called curtain air (CA). The CA flow rate is controlled by a separate mass flow controller and the air is preheated electrically. This FI configuration can be seen as representing a simplified single injection point of a multiple point FI that is typically used in gas turbine combustors. The FI was installed $l_1 = 150\,\text{mm}$ upstream of the backward facing step of the sequential combustor in configuration 1 and

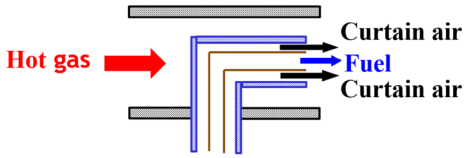


**Fig. 2:** Schematic of the inline fuel and curtain air injector.

$l_2 = 100\,\text{mm}$ in configuration 2 respectively (see fig. 3). The injector had an inner diameter of 6.5 mm (fuel jet) and the outer diameter of the cylindrical FI part at the outlet was 13 mm. The residence times in the MS were in the range of 1 to 0.4 ms, typical for a practical system.

An emission probe at the inlet of the MS serves to characterize the exhaust gas composition of the HG. About 70 mm downstream of the emission probe, a thermocouple (TC) probe was installed to measure the temperature of the hot gas at the axis of symmetry at the inlet of the sequential combustor T-$SC_{in}$. This TC was in relation to [3] newly designed for the experiments with configuration 2 in order to simplify its regular replacement. The probe was designed as a shielded cylindrical probe with a flow passage in which the hot gas temperature is measured with a K-type TC. The outer surface of the probe was made of zirconium oxide ceramics in order to minimize heat losses.

The MS has a cross section of $25 \times 25\text{mm}^2$ and a total length of 310 mm. The FI exit defines the position $x = 0\,\text{mm}$. The last 25 mm prior the sudden expansion were optically not accessible.

The SC has a cross section of 70 x 70 $\text{mm}^2$ and was 170 mm long. The window in the SC has an axial width of 31 mm (see fig. 3). The converging section towards the exit of the SC was implemented for the $H_2$ injection experiments performed within the scope of the FLEX4H2 project and differs from the original configuration studied in 2015.

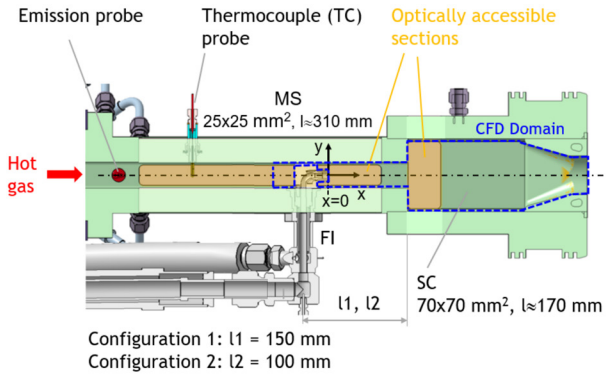


**Fig. 3:** Sketch of the mixing section (MS) and the sequential combustor (SC).

Due to the sharp transition in flow area from the MS to the SC, recirculation zones are typically present in the corners of the SC close to the mixing duct exit. In this work, we focus on the second stage burner (MS and injector) and the SC sketched in fig. 3.

Auto-ignition kernels in the MS observed in the configuration 1 experiments were detected by recording the flame luminosity signal with a high-speed camera of a recording rate of up to 30 kHz (see [6] for details). In the $H_2$ flame experiments (configuration 2), the heat release zone in the SC was studied using OH* chemiluminescence (CL) measurements. The OH*-CL signal was detected with two cameras at few Hz repetition rates, one from the top and one from the side, and 400 single shot images were averaged to obtain the mean flame position. In addition, high-speed OH*-CL imaging was applied to evaluate the AI and flame stabilization behavior. As a compromise, a recording rate of 5 kHz was used in these measurements in order to allow the observation of a larger field of view (mixing zone and first part of SC) and still have a manageable size of the kHz videos.

## 2.2 Numerical solver

We solve the coupled set of partial differential equations describing multi-component turbulent reacting flow, comprising the Favre-filtered balance equations for mass, momentum, and energy. A dynamic one-equation subgrid-scale eddy viscosity model [19] is solved to evaluate the filter coefficients in the LES formulation. The detailed chemical reaction kinetics scheme developed at Princeton university, considering 9 species and 21 elementary reactions to describe hydrogen-oxygen combustion [20], is used in the LES calculations (excluding nitrogen- and carbon-species reactions). Consequently, in the numerical simulations, for efficiency of the solution, we have replaced the $CO_2$ formed in the hot gas generator with $H_2O$ to avoid introducing carbon species in the kinetics and transport equations. The open-source C++ libraries OpenFOAM-12 are used in this work. OpenFOAM is a generic, high fidelity, framework for finite-volume discretization of partial differential equations, including a high degree of user flexibility in terms of identifying and choosing mathematical formulations [21]. We have used the compressible, reactive, `reactingFoam` solver with dynamic load balancing and analytical Jacobian for the cell chemistry [22, 23]. While dynamic load balancing is not critical for the modest number of species in the Li mechanism, the enhanced stability provided by using an analytical Jacobian, combined with improved implementations for the linear algebra (LAPACK) and use of a semi-implicit extrapolation-based Euler method (Seulex) for solving the chemistry ODEs, is attractive for highly reactive hydrogen flames. Additionally, we employ the thermodynamically consistent `FickianTransportFoam` provided by [24], ensuring that non-unity Lewis number diffusivity effects are appropriately accounted for. The importance of correctly accounting for, e.g., enthalpy diffusion when aiming at predicting AI locations in hydrogen-air shear flows is highlighted by [25]. Further, the `FickianTransportFoam` model allows to specify inter-species diffusion coefficients for a range of pressures and temperatures, which are consistently agglomerated to provide the species' diffusion coefficient with respect to the mixture. A sketch of the CFD domain is contained in fig. 3, showing the outline of the mixing-section and the SC. Overall, the geometry consists of a narrow mixing channel, a wider combustor channel and the (fuel-) injector nozzles. The dimensions of the mixing duct in the downstream, span-wise, and vertical direction,

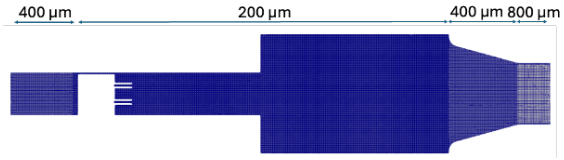


**Fig. 4:** Cross-cut view of the computational domain with grid cells and resolution.

are 148 × 25 × 25 mm$^3$, respectively. At the end of the mixing duct, the flow expands into the SC of dimensions 516 × 70 × 70 mm$^3$, respectively. The final third of the SC features a converging section towards the outlet.
Previous simulations of similar, but simplified, geometries have indicated that the physics of interest occur in the mixing duct, where the turbulence is developed and turbulent mixing needs to be accounted for, up to about the first third of the SC, where flame stabilization is expected [17]. Hence, the first part of the mixing section upstream of the FI is resolved at 400 µm, and the majority of the numerical effort is deployed around the FI in the mixing section and up to the converging part of the SC at 200 µm resolution. The volume bound by the converging part is resolved at 400 µm and the last part near the outlet at 800 µm, see fig. 4. Accordance with the Pope criterion [26] is ensured for the bulk flow where 70 to 80 % of the turbulent kinetic energy is represented by the resolved motions. The resulting computational domain encompasses 78 million mostly hexahedral cells. We limit the time-step by a maximum allowable Courant number of 0.6 in the PIMPLE algorithm (a hybrid SIMPLE-PISO iteration scheme) for pressure-velocity coupling. In the fully developed turbulent and reactive state, this corresponds to a numerical time step of approximately $1 \times 10^{-7}$ s. An implicit second order backward time integrator is used. Spatial operators are discretized by second order central differencing schemes. Massively parallel computations are performed on the UNINETT Sigma2 High Perfomance Computing cluster Betzy on 5120 CPUs.

## 2.3 Configuration and boundary conditions

Two configurations with different boundary conditions have been studied experimentally and numerically to investigate the effects of fuel reactivity and hot-gas temperature on flame stabilization. The first configuration with a lower fuel reactivity included $N_2$-diluted hydrogen injection with a low (case C1) and a high hydrogen flow rate (case C2). The operating conditions were almost the same in both cases (see Table 1). Configuration 1 was the starting point for the validation of the numerical simulations.
Pure hydrogen was injected in the second configuration (cases C3 to C5) which represents cases with a higher fuel reactivity. These three cases differ by the hot gas inlet temperature which was 64 K higher in case C5. The $H_2$ flow rates were the same (see Table 1 for details). The same FI but different FI positions were used in the two configurations to take into account the differences in the reactivity of the fuel air mixtures. As mentioned in chapter 2.1, a section with a converging inner diameter was installed in the SC for configuration 2 (cases C3 to C5) to exclude any interaction of the flow in the downstream exhaust gas piping with the SC.

Table 1: Experimental operating conditions.

| | C1 | C2 | C3 | C4 | C5 |
|---|---|---|---|---|---|
| Fuel | $H_2/N_2$ | $H_2/N_2$ | $H_2$ | $H_2$ | $H_2$ |
| Pressure | 15 | 15 | 10 | 10 | 10 |
| Normalized hot gas inlet temperature [-] | 1.055 | 1.052 | 1.024 | 1.068 | 1.084 |
| Fuel $H_2$ flow rate [g/s] | 2.9 | 4.1 | 5 | 5 | 5 |
| Fuel $N_2$ flow rate [g/s] | 31.5 | 32.5 | - | - | - |
| Curtain air mass flow rate [g/s] | 36.2 | 37.9 | 36.0 | 35.9 | 36.0 |
| Hot gas mass flow rate [g/s] | 605 | 620 | 390 | 365 | 360 |
| Fuel temperature at FI inlet [K] | 345 | 343 | 295 | 293 | 292 |
| Curtain air temperature at FI inlet [K] | 593 | 588 | 525 | 529 | 522 |

The hot-gas composition and temperature for the CFD are uniformly set according to plug-flow reactor calculations performed with Cantera [27] and compared with thermocouple measurements for consistency. However, it is expected that a temperature and compositional variance in the hot-gas flow is present in the experiments. This is caused by the method used for dilution-air addition to the products stream emerging from the first combustor where such dilution-air addition is implemented in the experiments by a geometrically complex tube-in-tube arrangement that cannot be practically represented in the numerical model. Consequently, the dilution air mixing with the hot gas takes place upstream of the region considered in the computational domain and the boundary condition for the hot gas assumes uniform mixture and temperature. Although this is a limiting assumption, it still allows to quantitatively evaluate the effect of hot-gas temperature and of the fuel reactivity (fraction of nitrogen dilution) on the flame stabilization process.

The thermal boundary conditions for injector walls, curtain-air and fuel streams are estimated from a conjugate heat transfer (CHT) simulation performed by Ansaldo Energia, using ANSYS Fluent. Mass flows through all inlets are ramped up to their respective mass values shown in Table 1 for 3 ms, respectively. During the ramp-up, reactions are not activated in the CFD. After the ramp-up is complete, the flow is allowed to develop for an additional 3 ms (approx. one fluid-parcel transit time through the domain), before reactions are activated. An overview of the boundary conditions is presented in Table 1. The thermal boundary conditions for the pure hydrogen cases are 853 K on the fuel channel and curtain air channel walls, and 973 K on the mixing section and fluid-facing injector walls, respectively. For the $N_2$-diluted cases, the fuel channel is at 420 K, curtain air inner channel at 480 K, curtain air outer channel at 805 K and the fluid-facing injector wall at 970 K, respectively. For case C1 and C2 the mixing section wall is kept at 970 K. The front panel and combustor walls are assumed to be adiabatic (zero heat flux). It should be noted that the

CHT calculations provide the thermal boundary conditions for the injector geometry only. The mixing section wall temperature is unknown, however, a thorough characterization of the mixing section has found that the applied external wall cooling resulted in a relatively modest heat loss of approximately 6 % [3].
The hot gas composition is assumed to be identical for both cases, with mass fractions according to $Y_{N_2} = 0.753$, $Y_{O_2} = 0.169$, and $Y_{H_2O} = 0.078$ (including $Y_{CO_2} = 0.04$), resulting from the first burner operated at equivalence ratio $\phi = 0.41$ and the added dilution air stream of 252 g/s. The far field pressure for the $N_2$ diluted hydrogen cases is 15 bar and 10 bar for the pure hydrogen cases. Inlets and material walls are effectively treated as zero flux, with the outlet provided a `waveTransmissive` boundary condition, allowing pressure waves to escape the domain in a non-reflective matter.

# 3 Results

## 3.1 Nitrogen diluted hydrogen flames

Auto-ignition and flame stabilization in the mixing section of $N_2$-diluted $H_2$ flames (configuration 1) were studied in the past for a wide range of inlet conditions and hydrogen fuel flow rates [7]. Due to the extremely fuel-lean operating conditions, a steady-state flame in the sequential combustor was rarely observed in these experiments. However, AI events in the mixing section were often observed and at some operating conditions even flame stabilization at the FI exit was found. From the extensive experimental database two cases (C1 and C2) were selected to serve as starting point for the validation of numerical simulations. As an example, flame luminosity images extracted from a kHz series are shown in fig. 5.

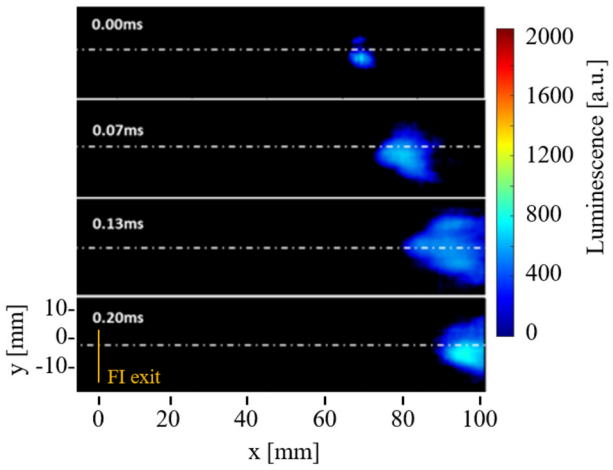


**Fig. 5:** Development of AI kernels illustrated by sequence of flame luminosity images extracted from a high-speed video (case C1).

The onset of an AI kernel is visible in the first image. As a definition, the time is set to $t = 0$ ms, when an AI kernel is detected the first time. From the following three images

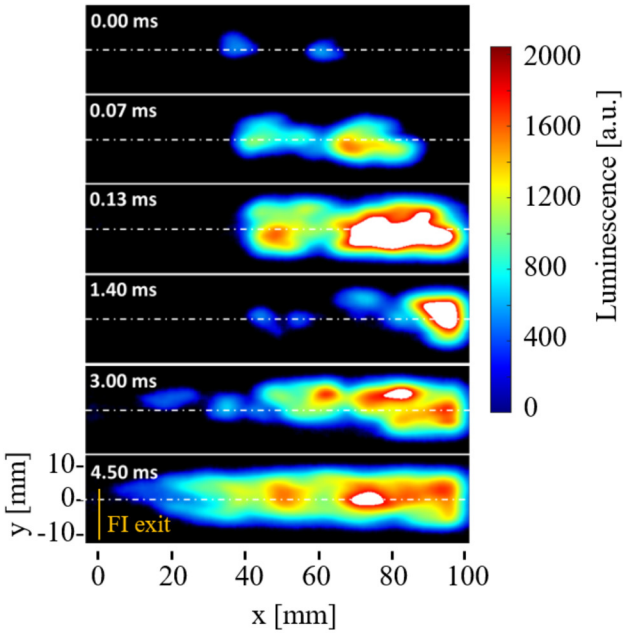


**Fig. 6:** Development of AI kernels and flame stabilization (FS) illustrated by sequence of flame luminosity images extracted from a high-speed video (case C2).

($t = 0.07 - 0.2$ ms) it is obvious that this kernel is growing in size and intensity, while it is transported downstream. This downstream convection is related to the local flow velocity in the mixing section, which in this case is higher than the local turbulent flame speed. For case C1, several AI events have been observed. None of these events triggered flame stabilization at the FI. In contrast, case C2 shows an example of flame stabilization at the FI (see fig. 6).

At the beginning of the sequence at $t = 0$ ms, two AI kernels were formed, which grow in size and intensity, while transported downstream. Subsequent kernels form further upstream and eventually merge with each other or with their predecessors. Two effects can be identified:
Firstly, a given kernel grows in size during its downstream movement. Due to local heat release and flame propagation, the trailing edge moves upstream relative to the kernel center of gravity, and eventually also in terms of absolute mixing section coordinates. Absolute upstream movement of the trailing edge occurs very rarely. Overall, the downstream movement of the kernel is dominating, which clearly illustrates that upstream flame propagation only occurs locally, limited to the close vicinity of the kernel boundaries. This is in agreement with findings in [28] and [29], who also report on the convective transport of local ignition spots with the main flow and kernel edge propagation only occurring locally. Subsequent AI kernels only form upstream of their predecessors at smaller $x$-positions closer to the injector exit plane at $x = 0$ mm. This indicates that the flame stabilization mechanism in this case is AI driven, and not due to upstream flame front propagation.
The second effect is the merging of kernels with their respective successors, given that these kernels form sufficiently close to each other. As explained, local flame

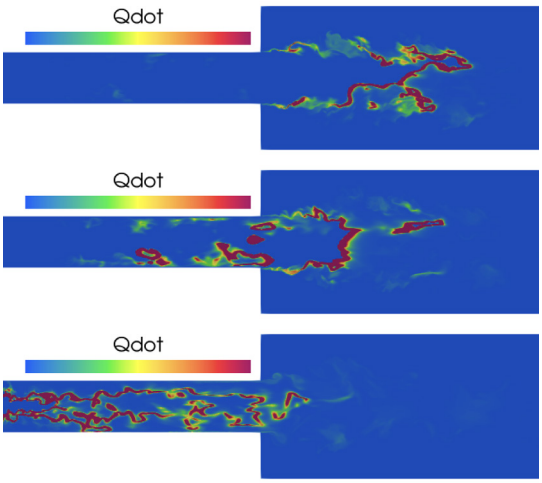


**Fig. 7:** CFD results for case C2, showing the development of AI kernels and flame stabilization (FS) illustrated by sequence of heat-release rate contours. The images are time-separated by 0.2 ms.

propagation limited to the close proximity of the kernel boundaries and the downstream movement of the succeeding kernels, can lead to the merging of several kernels into one larger entity (see fig. 6, $t = 0.07 - 0.13$ ms). At this instant ($t = 0.13$ ms), the mixing section is at least in the vertical direction fully blocked by this entity. This is important for the following time intervals, in which more AI kernels are formed due the local conditions in favor of AI due to a locally higher inlet temperature and a locally lower flow velocity caused by this mixing section blockage. The locally higher inlet temperature is caused by the heat release of the merged kernels ($t = 1.4 - 3$ ms). The end of the sequence is characterized by the development of the last succeeding kernel and its merging with its predecessors, which are still present in the mixing section, and the subsequent stabilization of the flame at the FI ($t = 4.5$ ms). Due to the kernel merging, the trailing edge moves upstream and the flame stabilizes at a certain lift-off height from the injector exit plane ($x = 0$ mm) due to the local balance between flame propagation speed and flow velocity.

Comparison with numerical results is offered in fig. 7. Here, case C2 has been simulated, yielding a stable flame, anchored at the tip of the backward-facing step, and positioned around 20 mm into the SC (cf. fig. 7 (top)). Subsequently, the hot gas temperature was increased by 200 K beyond the mean temperature value measured in the experiments. This mimics high-frequency temperature (and composition) fluctuations possibly induced by the dilution air mixing with the hot gas in the experiments that are not resolved by the thermo-couple providing the reference conditions. When the increased temperature is advected downstream of the injector nozzle, small AI kernels are observed also in the CFD results(fig. 7 (middle)). Similar to the experimental observations (fig. 6), the flame quickly attaches at the FI, fig. 7 (bottom).

## 3.2 Pure hydrogen flames

Results of the $H_2$ flames (configuration 2, cases C3 to C5 are discussed using fig. 8, fig. 9 and fig. 10.
In the experiments with pure $H_2$, the SC was operated as follows: the first stage combustor (HG) was ignited and the HG operating conditions (pressure, inlet temperature, equivalence ratio) were ramped up to targeted values for the ignition of the SC. Afterwards, $H_2$ was injected in the MS and the SC was ignited with the help of an ignition laser. The laser ignition was used in order to allow a safe, soft and controlled ignition without risking a hardware damage due to a violent and uncontrolled ignition. After a steady-state flame has been settled, the SC operating conditions (pressure, inlet temperature, $H_2$ flow rate resp. equivalence ratio) are adjusted to the targeted values. The experiments were performed with different SC inlet temperatures until flame stabilization at the FI was observed to evaluate the operational limits.
Top views of the averaged heat release zones, represented by the OH*-CL signal distribution averaged over 400 images are presented in fig. 8 (top left) and fig. 9 (top figure). In the sequential combustor a lifted steady-state flame was observed in the experiments. The lift-off height is about 20 mm from the $x$-position of the sudden expansion. Due to the limited optical access, only the flame root is visible. A side view of contours of the averaged heat-release rate obtained from the numerical simulations is shown in fig. 8 (top right).
Large axial flame fluctuations are observed in the experiments. The fluctuation of the heat release zone is visible from the images in fig. 8 (bottom left) and fig. 9 (bottom). Top views of the standard deviation of the OH*-CL signal are shown. Although the flame sometimes appears in the last part of the mixing section, the flame does not propagate further upstream. In other words, at these operating conditions no flame stabilization at the fuel injector was observed. However, the conditions of case C4 results would be potentially risky for a GT operation. The experimental imaging of the flame is based on OH*-CL signal that is line-of-sight integrated (by the camera sensor) while the numerical results show the heat-release rate on a two-dimensional slice of the computational domain. This fundamental difference in the diagnostic method results in the observed visual difference that, however, does not imply any disagreement about the flame-stabilization process. The two-dimensional slice of the heat-release rate field clearly indicate the occurrence of thin propagating flame fronts closer to the corners of the backward-facing step and thicker auto-igniting regions in the bulk flow. Line of sight integration of the heat-release rate spatial pattern is compatible with the OH*-CL measurements.

In summary, at these operating conditions the experimental results show a lifted steady-state flame with large axial fluctuations but without a flame stabilization at the FI.

Experiments to evaluate flame stabilization are performed by a slow stepwise increase of the $H_2$ flow rate at constant pressure and inlet temperature. After each step, a pause of several minutes is applied to see whether flame an-

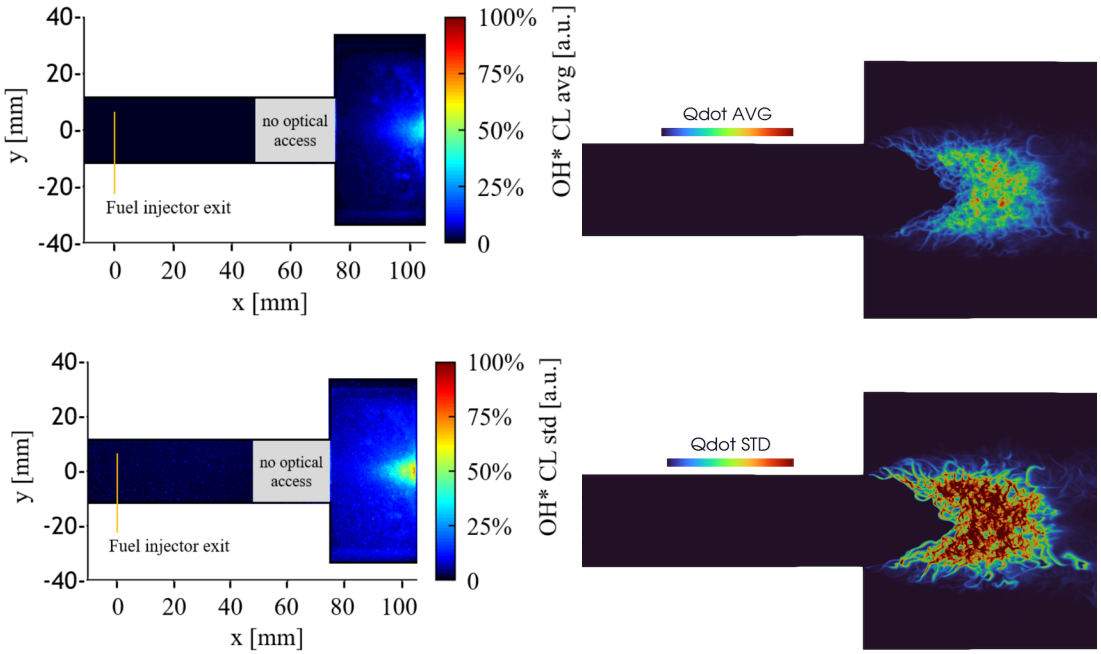


**Fig. 8:** Comparison of experimental (left) and simulations results (right) for $H_2$ flames (configuration 2, case C3). Averaged flame position (top images) and fluctuation of heat release zone (bottom images).

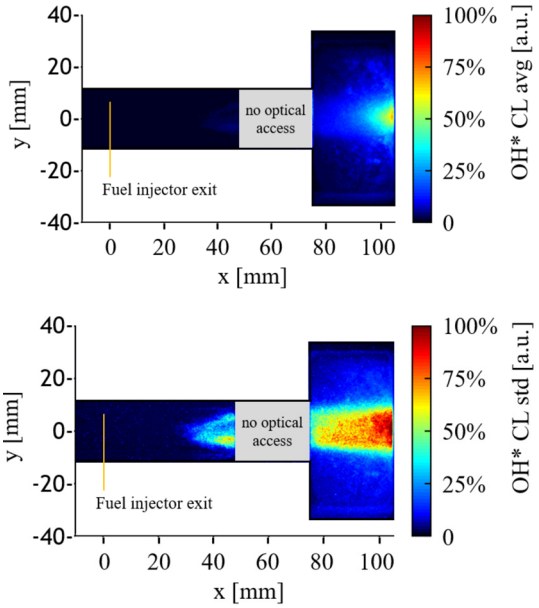


**Fig. 9:** Configuration 2, case C4 experiments: Averaged (top) and fluctuating heat release (bottom).

choring at the FI occurs or not. If no flame stabilization at the FI occurred, the next $H_2$ flow rate step was introduced. As an example of an event triggering flame stabilization at the FI exit, in fig. 10 a sequence of OH*-CL images extracted from a kHz series is shown. The flame stabilizes at the fuel injector at $t_{FS}$. Five images corresponding to different times are presented. In the top image at $t_{FS} - 0.6$ ms the leading edge of the flame is located at $x \approx 40$ mm, close to the end of the optically accessible part of the mixing section. In the following time interval of 0.4 ms (from $t_{FS} - 0.6$ to $t_{FS} - 0.2$ ms) the flame leading edge rapidly propagates upstream until it stabilizes at the FI at $t_{FS}$. A visual estimation of the instantaneous upstream displacement of the flame edge gives a relative velocity of $\approx$ 150 m/s, which is of the order of the underlying MS flow velocity. This implies a displacement speed of $\approx$ 300 m/s excluding that flame propagation is alone able to control flame stabilization. A similar process is observed in the CFD results, with rapid upstream displacement of the flame finally anchoring at the FI, cf. fig. 10 (right column).

## 4 Conclusions

Novel results from experimental and numerical investigations of $N_2$-diluted $H_2$ flames and pure $H_2$ flames in a laboratory-scale SC at high pressure were presented.
For the $N_2$-diluted $H_2$ flames, the formation of downstream advected AI kernels is observed at lower $H_2$ flow rates. At higher $H_2$ flow rates, kernel merging aids in the upstream flame propagation, leading to flame anchoring at the FI. The numerical simulations correctly predict a stable flame in the SC for lower $H_2$ flow rates. The formation of larger AI kernels in the mixing section prior to rapid flame anchoring at the FI for higher $H_2$ flow rates, is reproduced by the numerical simulations for reasonably elevated hot gas inlet temperatures, compared to the experimental conditions.
For the pure $H_2$ experiments, stable flames were observed for lower hot gas inlet temperature. Flame stabilization at the FI was observed for increased hot gas temperature. The numerical model is able to capture stable operation at the lower temperature conditions, whence rapid transition to flame anchoring at the FI is found in the numerical simulations for elevated hot gas temperature, compared to the experimental conditions. The sporadic AI events observed in the experiments are generally not captured by the numer-

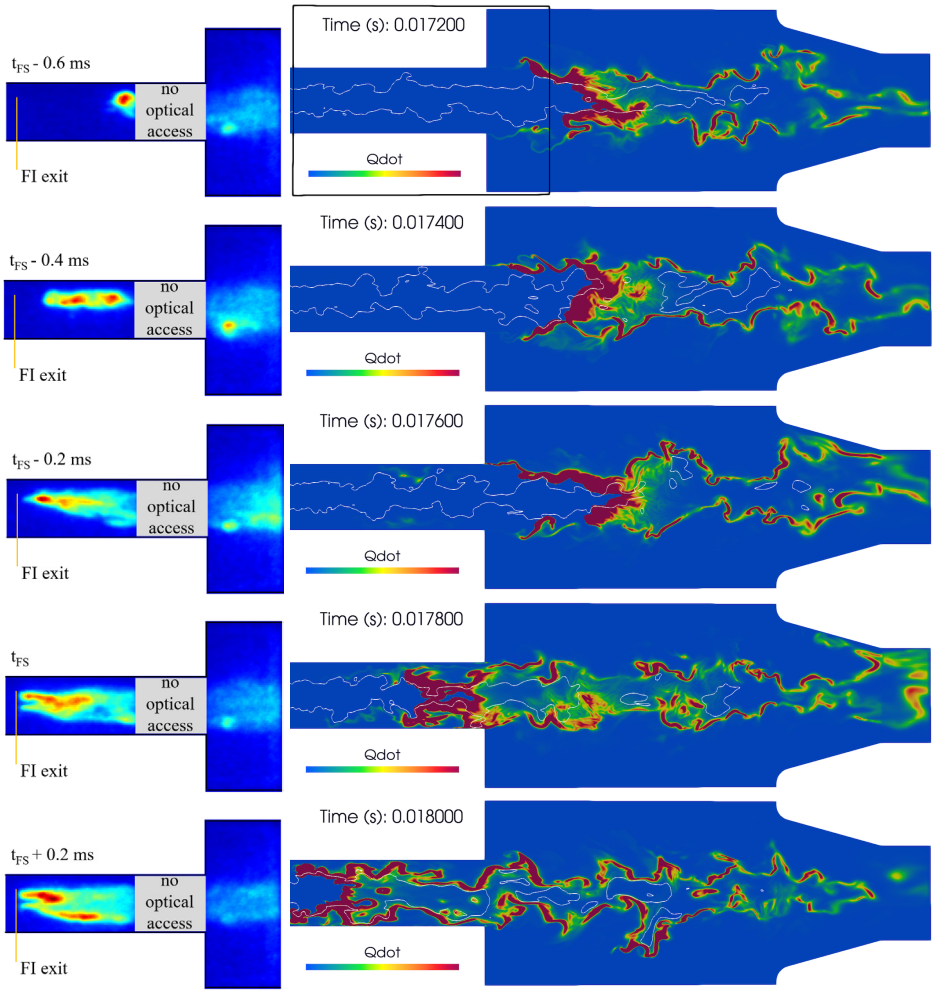


**Fig. 10:** Comparison of experimental and simulated results of configuration 2, case C5. Flame stabilization event at FI illustrated by sequence of OH*-CL images extracted from a high-speed video (left) and color contours of CFD heat-release rate together with the stoichiometric $H_2$ mass fraction contour (right). The top right picture indicates the experimental measurement domain by the black outline.

ical model, this shortcoming is explained by the absence (in the numerical model) of the compositional and temperature variance present in the hot gas downstream of the dilution air injection location. This aspect will be investigated in future work.

## ACKNOWLEDGEMENTS

The numerical work and the experimental work on $H_2$ injection were performed within the scope of the FLEX4H2 project. The FLEX4H2 project is supported by the Clean Hydrogen Partnership and its members European Union, Hydrogen Europe and Hydrogen Europe Research (GA 101101427), and the Swiss Federal Department of Economic Affairs, Education and Research, State Secretariat for Education, Research and Innovation (SERI). Views and opinions expressed are however those of the author(s) only and do not necessarily reflect those of the European Union or any other granting authority. Neither of them is liable for any use that may be made of the information contained therein.

The experimental work on $H_2/N_2$ mixtures has been funded by Ansaldo Energia and the German Federal Ministry for Economic Affairs and Energy within the AG Turbo 2020 Research Program, as well as by DLR basic funding which is gratefully acknowledged.
The computational and data storage allocation, granted to the authors by UNINETT Sigma2 - the National Infrastructure for High Performance Computing and Data Storage in Norway (project number nn8035k and ns8035k), made this study possible.

## References

[1] Güthe, F., Hellat, J., and Flohr, P., 2009. "The reheat concept: the proven pathway to ultra-low emissions and high efficiency and flexibility". *Journal of Engineering for Gas Turbines and Power,* ***131***, p. 021503.

[2] Wind, T., Güthe, F., and Syed, K., 2014. "Co-firing of hydrogen and natural gases in lean premixed conventional and reheat burners (Alstom GT26)". In Proceedings of ASME Turbo Expo: Power for Land, Sea and

Air, June 16-20 2014, Düsseldorf, Germany, ASME, pp. GT2014–25813.

[3] Fleck, J., Griebel, P., Steinberg, A. M., Stöhr, M., Aigner, M., and Ciani, A., 2010. "Experimental investigation of a generic, fuel flexible reheat combustor at gas turbine relevant operating conditions". In Proceedings of ASME Turbo Expo: Power for Land, Sea and Air, June 14-18 2010, Glasgow, Scotland, ASME, pp. GT2010–22722.

[4] Fleck, J., Griebel, P., Steinberg, A. M., Stöhr, M., Aigner, M., and Ciani, A., 2012. "Autoignition Limits of Hydrogen at Relevant Reheat Combustor Operating Conditions". *Journal of Engineering for Gas Turbines and Power,* ***134***, p. 041502.

[5] Fleck, J. M., Griebel, P., Steinberg, A. M., Arndt, C. M., Naumann, C., and Aigner, M., 2013. "Autoignition of hydrogen/nitrogen jets in vitiated air crossflows at different pressures". *Proceedings of the Combustion Institute,* ***34***(2), pp. 3185–3192.

[6] Schmalhofer, C., Griebel, P., Stöhr, M., and Aigner, M., 2015. "Auto-ignition of in-line injected hydrogen/nitrogen fuel mixtures at reheat combustor operating conditions". In Proceedings of the ASME Turbo Expo: Power for Land, Sea and Air, ASME, pp. GT2015–43414.

[7] Schmalhofer, C., Griebel, P., and Aigner, M., 2018. "The influence of carrier air preheating on autoignition of inline-injected hydrogen-nitrogen mixtures in vitiated air of high temperature". *Journal of Engineering for Gas Turbines and Power,* ***140***, p. 031502.

[8] Poyyapakkam, M., Wood, J., Mayers, S., Ciani, A., Güthe, F., and Syed, K., 2012. "Hydrogen combustion within a gas turbine reheat combustor". In Proceedings of ASME Turbo Expo: Power for Land, Sea and Air, June 11-15 2012, Copenhagen, Denmark, ASME, pp. GT2012–69165.

[9] Brower, M., Petersen, E., Metcalfe, W., Curran, H., Füri, M., Bourque, G., Aluri, N., and Güthe, F., 2013. "Ignition delay time and laminar flame speed calculations for natural gas/hydrogen blends at elevated pressures". *Journal of Engineering for Gas Turbines and Power,* ***135***, pp. 021504–1–10.

[10] Aditya, K., Gruber, A., Xu, C., Lu, T., Krisman, A., Bothien, M., and Chen, J., 2019. "Direct numerical simulation of flame stabilization assisted by autoignition in a reheat gas turbine combustor". *Proceedings of the Combustion Institute,* ***37***(2), pp. 2635–2642.

[11] Schulz, O., Jaravel, T., Poinsot, T., Cuenot, B., and Noiray, N., 2017. "A criterion to distinguish autoignition and propagation applied to a lifted methane–air jet flame". *Proceedings of the Combustion Institute,* ***36***(2), pp. 1637–1644.

[12] Schulz, O., and Noiray, N., 2018. "Autoignition flame dynamics in sequential combustors". *Combustion and Flame,* ***192***, pp. 86 – 100.

[13] Yang, Y., Noiray, N., Scarpato, A., Schulz, O., Düsing, K. M., and Bothien, M. R., 2015. "Numerical analysis of the dynamic flame response in alstom reheat combustion systems". In Proceedings of ASME Turbo Expo: Power for Land, Sea and Air, June 15-19 2015, Montreal, Canada, ASME, pp. GT2015–42622.

[14] Scarpato, A., Zander, L., Kulkarni, R., and Schuermans, B., 2016. "Identification of multi-parameter flame transfer function for a reheat combustor". In Proceedings of ASME Turbo Expo: Power for Land, Sea and Air, June 13-17 2016, Seoul, South Korea, ASME, pp. GT2016–57699.

[15] Bothien, M., Lauper, D., Yang, Y., and Scarpato, A. "Reconstruction and Analysis of the Acoustic Transfer Matrix of a Reheat Flame From Large-Eddy Simulations". *Journal of Engineering for Gas Turbines and Power,* ***141***, p. 021018.

[16] Gruber, A., Bothien, M. R., Ciani, A., Aditya, K., Chen, J. H., and Williams, F. A., 2021. "Direct numerical simulation of hydrogen combustion at autoignitive conditions: Ignition, stability and turbulent reaction-front velocity". *Combustion and Flame,* ***229***, p. 111385.

[17] Gruber, A., Heggset, T., Duesing, M., and Ciani, A., 2022. "A numerical investigation of reheat hydrogen combustion in a simplified geometrical configuration from atmospheric pressure to full load conditions". In Proceedings of ASME Turbo Expo: Power for Land, Sea and Air, June 13-17, 2022, Rotterdam, The Netherlands, ASME, pp. GT2022–83218.

[18] Gruber, A., Meyer, O. H. H., Heggset, T., Wood, B., and Ciani, A., 2024. "Numerical Investigation of Reheat Hydrogen Flames in the Sequential-Combustion Stage of a Heavy-Duty Gas Turbine". In Proceedings of ASME Turbo Expo: Power for Land, Sea and Air, June 24-28, 2024, London, United Kingdom, ASME, pp. GT2024–128966.

[19] Kim, W., and Menon, S., 1995. "A new dynamic one-equation subgrid-scale model for large eddy simulations". In 33rd Aerospace Sciences Meeting and Exhibit, AIAA.

[20] Li, J., Zhao, Z., Kazarov, A., and Dryer, F. L., 2004. "An updated comprehensive kinetic model of hydrogen combustion". *International Journal of Chemical Kinetics,* ***36***, pp. 566–575.

[21] Weller, H. G., Tabor, G., Jasak, H., and Fureby, C., 1998. "A tensorial approach to computational continuum mechanics using object-oriented techniques". *Computers in Physics,* ***12***, pp. 620–631.

[22] Tekgül, B., Peltonen, P., Kahila, H., Kaario, O., and Vuorinen, V., 2021. "Dlbfoam: An open-source dynamic load balancing model for fast reacting flow simulations in openfoam". *Computer Physics Communications,* ***267***, p. 108073.

[23] Morev, I., Tekgül, B., Gadalla, M., Shahanaghi, A., Kannan, S., Karimkashi, S., Kaario, O., and Vuorinen, V., 2022. "Fast reactive flow simulations using analytical jacobian and dynamic load balancing in openfoam". *Physics of Fluids,* ***34***, p. 021801.

[24] Rintanen, A., and Morev, I., 2025. Personal communication. Aalto University, Espoo, Finland, Feb.

[25] Cook, A., 2009. "Enthalpy diffusion in multicomponent flows". *Physics of Fluids,* ***21***, p. 055109.

[26] Pope, S. B., 2004. "Ten questions concerning the large-eddy simulation of turbulent flows". *New Journal of Physics,* ***6***, p. 35.

[27] Goodwin, D. G., Moffat, H. K., Schoegl, I., Speth, R. L., and Weber, B. W., 2024. Cantera: An object-oriented software toolkit for chemical kinetics, thermodynamics, and transport processes. `https://www.cantera.org`. Version 3.1.0.

[28] Markides, C. N., and Mastorakos, E., 2007. "Flame propagation following the autoignition of axisymmetric hydrogen, acetylene, and normal-heptane plumes in turbulent coflows of hot air". *Journal of Engineering for Gas Turbines and Power,* ***130***, p. 011502.

[29] Oldenhof, E., Tummers, M. J., van Veen, E. H., and Roekaerts, D. J. E. M., 2010. "Ignition kernel formation and lift-off behaviour of jet-in-hot-coflow flames". *Combustion and Flame,* ***157***, pp. 1167–1178.